ACS OMEGA

Open Access

http://pubs.acs.org/journal/acsodf

Article

Characterization, Preparation, and Promotion of Plant Growth of 1,3-Diphenylurea/β-Cyclodextrin Derivatives Inclusion Complexes

Koki Yamamoto, Takashi Tanikawa, Junki Tomita, Yoshiyuki Ishida, Daisuke Nakata, Keiji Terao, and Yutaka Inoue*

Cite This: *ACS Omega* 2023, 8, 34972−34981

Read Online

ACCESS | Metrics & More | Article Recommendations | Supporting Information

ABSTRACT: The study aimed to prepare inclusion complexes of 1,3-diphenylurea (DPU) with β-cyclodextrin (βCD) and 2-hydroxypropyl-β-cyclodextrin (HP-βCD) using a three-dimensional ground mixture (3DGM). Their physicochemical properties, intermolecular interactions, solubilities, and plant growth-promoting activities were investigated on broccoli sprouts. Phase-solubility diagrams indicated the stability constant (K_s) and complexation efficiency (CE) of βCD/DPU were found to be $K_{1/1}$ = 250 M^{-1}, CE = 2.48× 10^{-3}. The K_s and CEs of HP-βCD/DPU were found to be $K_{1/1}$ = 427 M^{-1}, CE = 3.93 × 10^{-3} and $K_{2/1}$ = 196 M^{-1}, CE = 1.93 × 10^{-3} respectively. The powder X-ray diffraction results of 3DGM (βCD/DPU = 2/1, HP-βCD/DPU = 2/1) showed that the diffraction peaks originating from the DPU and βCD disappeared, indicating a halo pattern. Differential scanning calorimetry results showed an endothermic peak at 244 °C derived from the melting point of DPU, but the endothermic peak disappeared in the 3DGM (βCD/DPU = 2/1, HP-βCD/DPU = 2/1). Near-infrared absorption spectra showed peak shifts in 3DGM (βCD/DPU and HP-βCD/DPU) at the −CH and −NH groups of DPU and the −OH groups of βCDs and free water. In the dissolution test (after 5 min), the concentration of intact DPU was 0.083 μg/mL. However, the dissolution concentrations of DPU in the 3DGM (βCD/DPU = 1/1), 3DGM (βCD/DPU = 2/1), 3DGM (HP-βCD/DPU = 1/1), and 3DGM (HP-βCD/DPU = 2/1) were 3.27, 3.64, 5.70, and 7.03 μg/mL, respectively, indicating higher solubility than that of the intact DPU. Further, ^{1}H−^{1}H NOESY NMR spectroscopic measurements showed cross-peaks between H-A (7.32 ppm) and H-B (7.12 ppm) of DPU and H-6 (3.79 ppm) in the βCD cavity of the 3DGM (βCD/DPU = 2/1). A cross-peak was also observed among DPU H-A (7.32 ppm), H-B (7.11 ppm), and H-6 (3.78 ppm) in the βCD cavity. The results of the broccoli sprout cultivation experiment showed that 3DGM (βCD/DPU = 1/1), 3DGM (βCD/DPU = 2/1), 3DGM (HP-βCD/DPU = 1/1), and 3DGM (HP-βCD/DPU = 2/1) increased the stem thickness compared with that of the control group (DPU). These results indicated that the βCD/DPU and HP-βCD/DPU inclusion complexes were formed by the three-dimensional mixing and milling method, which enhanced the solubility and plant growth-promoting effects.

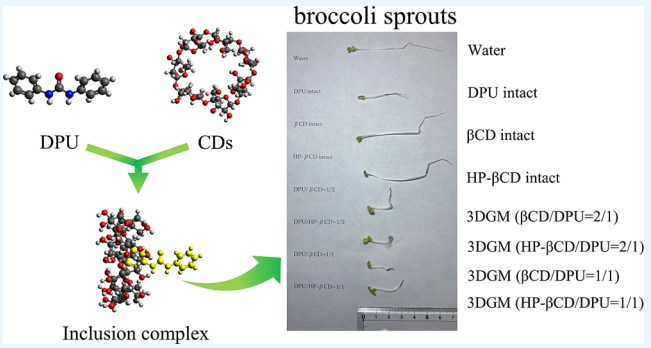

INTRODUCTION

Kinetin,[1] an adenine form of the plant hormone cytokinin, and forchlorfenuron (CPPU),[2] a form of phenyl urea, are effective agents for promoting plant growth. Cytokinins play diverse roles in plant growth, such as promoting cell division and germination,[3] preventing fruit loss and defoliation, improving fruit set,[4] and promoting nutrient uptake.[5] Further, CPPU, a phenylurea-based plant growth agent, is used in agricultural and horticultural sectors for fruit enlargement in grapes, apples, and kiwifruits.[6,7] Notably, 1,3-diphenylurea (DPU) is the basic framework matrix of phenyl urea-type cytokinin, and it independently acts as a cytokinin.[8] Owing to its poor solubility in water, it must be applied to plants using organic solvents. The use of organic solvents as plant growth agents poses challenges owing to their potential toxicity to plants and humans.[9−11] However, improved handling and solubility of DPU could lead to its use as a plant growth agent in various fields.

Cyclodextrin (CD) is a toroidal cyclic polysaccharide consisting of α-1,4-glycosidic linkages of D-glucopyranose. Depending on the number of glucopyranose units, it is classified as αCD, βCD, and γCD, comprising six, seven, and eight units, respectively,[12] each functioning as a host molecule to form inclusion complexes. Notably, CDs have hydrophobic inner cavities and hydrophilic outer rings.[13] Therefore,

Received: June 21, 2023
Accepted: September 4, 2023
Published: September 13, 2023

hydrophobic guest molecules can be encapsulated in the cavity via hydrogen bonding, van der Waals forces, hydrophobic interactions, and electrostatic attraction,[14] thereby improving the solubility[15] and stability[16] of the guest molecules. For example, inclusion complex formation between mefenamic acid (MA), a type of nonsteroidal anti-inflammatory drug, and βCD improves the solubility of MA.[15] In addition, the stability of doxycycline hyclate improves when it forms an inclusion complex with βCD.[16] Further, CD derivatives can be substituted with functional groups such as hydroxypropyl, methyl, hydroxyl, and sulfobutyl ether on the outer surface of CD. Notably, CD substituted with hydroxypropyl exhibits significant inclusion properties, high water solubility, and low toxicity toward many guest molecules.[17] In the field of food, the formation of an inclusion complex between curcumin, a polyphenolic compound contained in turmeric root, and 2-hydroxypropyl-β-cyclodextrin (HP-βCD) improves solubility and permeability via the gastrointestinal wall and blood−brain barrier.[18] In pharmaceuticals, inclusion complex formation between azithromycin (AZM), used to treat chronic periodontitis, and HP-βCD improves solubility of AZM.[19] Our previous study showed that the formation of inclusion complexes between CPPU and γCD or 2-hydroxypropyl-γ-cyclodextrin (HP-γCD) improved solubility and exhibited growth-promoting effects on plants.[20]

Inclusion complexes are prepared by grinding mixtures, a chemical reaction in mechanochemistry, with the application of mechanical forces to induce drug−drug interactions, leading to the inclusion of the guest drug in the CD cavity.[21] The advantage of this method is that inclusion complexes can be formed without using organic solvents and are therefore unaffected by oxidation, reduction, or hydrolysis.[22] Additionally, the three-dimensional mixed grinding method uses two rotational axes, allowing the entire inner surface of the spherical container to be utilized, which overcomes the disadvantages of two-dimensional mixed grinding methods, such as the heat produced during grinding and unevenness in mixing.[23] We previously reported the formation of inclusion compounds and improved solubility of rifampicin, an antibiotic, using βCD and γCD by the three-dimensional mixed grinding method.[24] In addition, the soybean components daidzein (DDZ) and genistein (GST) were prepared as DDZ/γCD and GST/γCD inclusion complexes by a three-dimensional mixed grinding method and improved solubility was reported.[25] Hence, if inclusion complexes of DPUs and CDs can be formed using a novel mixed grinding method involving three-dimensional mixing, DPUs and phenyl urea-type cytokinins, which are DPU derivatives, can provide basic information for improving the solubility of plant growth regulators.

Therefore, in this study, inclusion complexes of DPU and CDs were prepared by using the three-dimensional mixed grinding method, and their physicochemical properties, intermolecular interactions, and solubilities were investigated. Additionally, the plant growth-promoting activity was investigated using broccoli sprouts.

RESULTS AND DISCUSSION

Phase-Solubility Diagrams. The phase-solubility diagrams are a generalized method also based on the method of Higuchi and Connors et al. for predicting the complex formation of CDs and drugs in solution.[26,27] Phase-solubility diagrams were prepared based on the solubility changes of the βCD/DPU and HP-βCD/DPU inclusion complexes in solution to calculate stability constants and to predict inclusion molar ratios (Figure 1). The solubility diagram is classified into

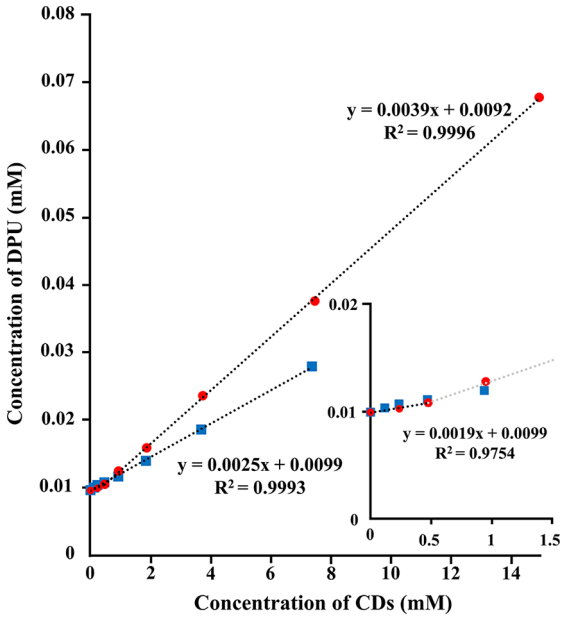

Figure 1. Phase-solubility diagram of βCD/DPU and HP-βCD/DPU. Results were expressed as mean ± SD (n = 3).

two types: type A (soluble complex) and type B (insoluble complex), with type A represented by A_L (linear diagram), A_P (positive deviation from linearity), and A_N (negative deviation from linearity) and type B by B_S (the complex has limited solubility) and B_I (the complex is insoluble).[27] The solubility of DPU in the phase-solubility diagram study was 2.14 ± 0.02 μg/mL (25 °C, D.W). In HP-βCD/DPU, the phase diagram showed an A_P type phase diagram, which deviated positively from the slope of the linear line as the HP-βCD concentration increased. On the other hand, for βCD/DPU, the linear diagram (A_L) type phase diagram showed a linearity up to a certain molar concentration range. According to Loftsson et al., when the slope of the linear A_L diagram is less than 1, the inclusion molar ratio of guest molecules to CD is 1/1, and when the A_P diagram is shown, the inclusion molar ratios are 1/1 and 1/2 in solution.[28] Therefore, the inclusion molar ratios of βCD/DPU = 1/1 and HP-βCD/DPU = 1/2 in the solution state are presumed to be βCD/DPU = 1/1 and HP-βCD/DPU = 1/2, respectively. The stability constants (K_s) and complexation efficiencies (CEs) of βCD/DPU and HP-βCD/DPU were calculated using the method described by Higuchi et al.[26] The K_s and CEs of βCD/DPU were found to be $K_{1/1}$ = 250 M^{-1}, CE = 2.48× 10^{-3}. The K_s and CEs of HP-βCD/DPU were found to be $K_{1/1}$ = 427 M^{-1}, CE = 3.93 × 10^{-3} and $K_{2/1}$ = 196 M^{-1}, CE = 1.93 × 10^{-3} respectively. At low values of the stability constant, the interaction between the guest molecule and the CD is weak; at values above 1000 M^{-1}, the interaction is strong, and the inclusion compounds do not readily dissociate.[29] For example, the stability constant of the adamantane/insulin conjugate-PEG-βCD complex is as high as 1.0 × 104 M^{-1}, indicating high retention without dissociation of the complex in blood.[30] However, the $K_{1/1}$ stability constant of βCD/DPU is lower than that of HP-βCD/DPU and comparable to that of $K_{2/1}$ of HP-βCD/DPU, suggesting that

https://doi.org/10.1021/acsomega.3c04428
ACS Omega 2023, 8, 34972−34981

βCD/DPU has characteristics that make it susceptible to dissociative properties.

Powder X-ray Diffraction (PXRD). PXRD analyses of βCD/DPU and HP-βCD/DPU were performed to investigate the changes in the crystal state of the solid dispersions (Figure 2). Characteristic diffraction peaks of the intact DPU were

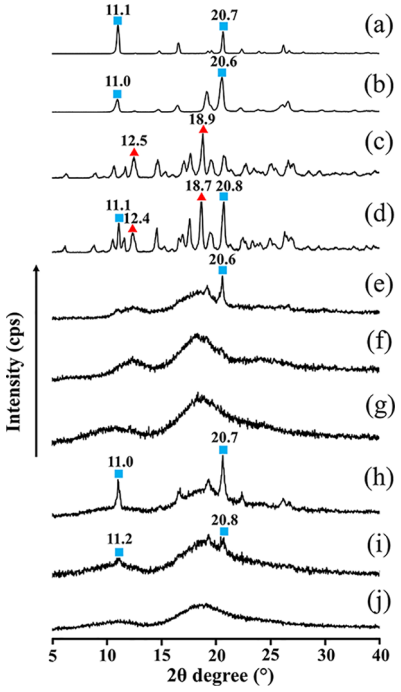

Figure 2. PXRD patterns of DPU intact, βCD/DPU and HP-βCD/DPU systems. (a) DPU intact, (b) DPU ground, (c) βCD intact, (d) PM (βCD/DPU = 2/1), (e) 3DGM (βCD/DPU = 1/1), (f) 3DGM (βCD/DPU = 2/1), (g) HP-βCD intact, (h) PM (HP-βCD/DPU = 2/1), (i) 3DGM (HP-βCD/DPU = 1/1), and (j) 3DGM (HP-βCD/DPU = 2/1). Blue solid square: DPU original; red solid triangle: βCD original.

observed at 2θ = 11.1 and 20.7° (Figure 2a) and those of the ground DPU were observed at 11.0 and 20.6° (Figure 2b). The characteristic peaks of the intact βCD were observed at 2θ = 12.5 and 18.9° (Figure 2c). In the physical mixture (PM; βCD/DPU = 2/1), the characteristic diffraction peaks of DPU were observed at 2θ = 11.1 and 20.8° and that of βCD at 12.4 and 18.7° (Figure 2d). In the three-dimensional ground mixture (3DGM) (βCD/DPU = 1/1), a DPU-derived diffraction peak was observed at 2θ = 20.6° (Figure 2e); however, in the 3DGM (βCD/DPU = 2/1), the characteristic DPU and βCD peaks disappeared, and a halo pattern was observed (Figure 2f). Incidentally, intact HP-βCD also showed a halo pattern (Figure 2g). In the PM (HP-βCD/DPU = 2/1), the characteristic diffraction peaks of DPU original were observed at 2θ = 11.0 and 20.7°; in the 3DGM (HP-βCD/DPU = 1/1), they were observed at 2θ = 11.2 and 20.8° (Figure 2h,i). In contrast, the 3DGM (HP-βCD/DPU = 2/1) exhibited a halo pattern (Figure 2j). Further, co-milling can cause disorders owing to the breakdown of the crystalline structure, and these amorphous solids exhibit a halo pattern.[31] In addition, the mechanochemical energy generated by milling and friction is likely to form amorphous inclusion complexes.[32] Notably, in the solid state, the formation of inclusion complexes via mixed milling was inferred to occur at a molar ratio of 2/1 for both 3DGM (βCD/DPU) and 3DGM (HP-βCD/DPU). From the phase-solubility diagram results, we initially hypothesized that βCD/DPU and HP-βCD/DPU formed inclusion complexes in a 1/1 ratio. However, we speculate that the inclusion molar ratios can differ between those of the solution and solid states.

Differential Scanning Calorimetry (DSC). The results of the PXRD analyses suggested the formation of 3DGM (βCD/DPU = 2/1, HP-βCD/DPU = 2/1) inclusion complexes in the solid state. Therefore, DSC analyses were performed to determine the thermal behavior of 3DGM (βCD/DPU, HP-βCD/DPU) (Figure 3). The peak at 244 °C was observed to

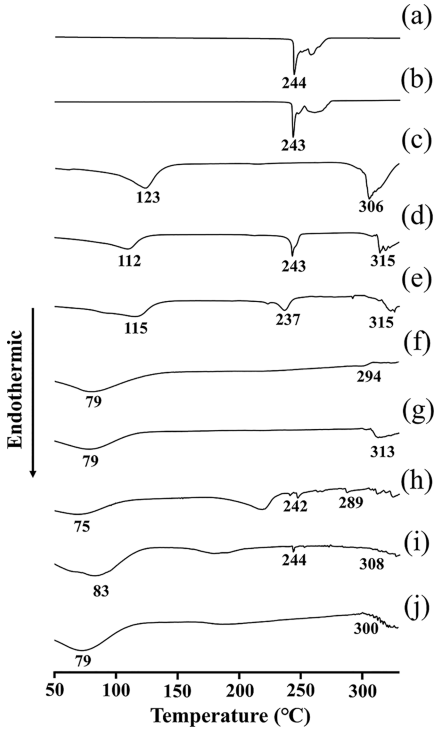

Figure 3. DSC corves of DPU intact, βCD/DPU and HP-βCD/DPU systems. (a) DPU intact, (b) DPU ground, (c) βCD intact, (d) PM (βCD/DPU = 2/1), (e) 3DGM (βCD/DPU = 1/1), (f) 3DGM (βCD/DPU = 2/1), (g) HP-βCD intact, (h) PM (HP-βCD/DPU = 2/1), (i) 3DGM (HP-βCD/DPU = 1/1), and (j) 3DGM (HP-βCD/DPU = 2/1).

be an endothermic peak due to the melting of DPU and the accompanying peak of DPU decomposition (Figure 3a), and the ground DPU indicated an endothermic peak owing to its melting at approximately 243 °C (Figure 3b). The βCD indicated an endothermic peak due to the dehydration of adsorbed water at approximately 123 °C; a peak was observed due to the decomposition of βCD at approximately 306 °C (Figure 3c). The PM (βCD/DPU = 2/1) indicated an endothermic peak owing to the DPU at approximately 243 °C. Further, an endothermic peak was observed owing to βCD at approximately 112 °C, and the peak of decomposition was observed at approximately 315 °C (Figure 3d). The peak at 237 °C in the 3DGM (βCD/DPU = 1/1) was observed to have an endothermic peak due to the melting of DPU. In addition, a peak of decomposition by βCD or βCD/DPU was observed around 290−315 °C (Figure 3e). In contrast, the 3DGM (βCD/DPU = 1/2) indicated the disappearance of a DPU-derived endothermic peak (Figure 3f). In HP-βCD

https://doi.org/10.1021/acsomega.3c04428
ACS Omega 2023, 8, 34972−34981

intact, a decomposition peak was observed around 313 °C (Figure 3g). In the PM (HP-βCD/DPU = 2/1), the endothermic peak due to DPU was observed at around 242 °C and the degradation peak due to βCD was observed at around 289 °C (Figure 3h). Similarly, in (Figure 3i) 3DGM (DPU/HPβCD = 1/1), an endothermic peak due to the melting of DPU was observed around 244 °C. Above 300 °C, a peak of decomposition due to HPβCD or DPU/HPβCD was observed. On the other hand, in 3DGM (βCD/DPU = 2/1), the endothermic peak due to DPU disappeared (Figure 3j). Typically, the disappearance of endothermic peaks, the appearance of new peaks, and the shifting and broadening of peaks are observed upon the inclusion complex formation.[33] Accordingly, the disappearance of the endothermic peaks due to the melting of the DPU was caused by both 3DGM (βCD/DPU) and 3DGM (HP-βCD/DPU) in the solid state via the formation of inclusion complexes at a molar ratio of 2/1. Initially, we considered that the inclusion molar ratio of βCD/DPU is 1/1 based on the phase-solubility diagrams of βCD/DPU. Therefore, in the solid state, βCD/DPU is thought to form inclusion complexes at a molar ratio of 1/1, and the preparation was carried out at a mixing ratio of βCD/DPU = 1/1. However, based on solid-state property evaluations such as XRD and DSC, it was found that the appropriate molar ratio was not βCD/DPU = 1/1 but βCD/DPU = 2/1. In other words, it was inferred that the inclusion status of βCD/DPU is different in the solution and solid state. Alternatively, βCD/DPU may also form an inclusion molar ratio of 2/1 in solution, but the complex may be dissociable. Interestingly, in the solid state, the CDs/DPU inclusion molar ratio of 2/1 was confirmed as a unique phenomenon. One possible reason for this is the 3D ball mill used in this preparation[23,24]. This 3D ball mill is a ball mill with two rotation axes (vertical and horizontal) like a gyro-mill because it is a ground mixture method in a 3D space. Interestingly, when the rotation of the two axes is adjusted, the balls move in random directions, making it possible to use the entire container for efficient milling. In other words, mechanochemical properties contribute to inclusion formation using the mixing and milling method in the solid state without solvent, and we are convinced that unique findings were discovered in this study.

Near-Infrared (NIR) Absorption Spectrum. The results of PXRD and DSC indicated that βCD/DPU and HP-βCD/DPU in the solid state formed inclusion complexes at a molar ratio of 2/1, respectively. Therefore, in order to confirm the intermolecular interactions of βCD/DPU and HP-βCD/DPU in the solid state, NIR absorption spectroscopy, an analysis in which detection is useful with respect to the −CH, NH, and OH groups, was performed[34] (Figure 4,5). The CH-derived peaks of the benzene rings in DPU were identified at 8787 and 5967 cm^{-1}, and similar peaks were identified in ground DPU (Figure 4a,c). The 3DGM (βCD/DPU = 2/1) showed broadening of both CH peaks of the DPU-derived benzene ring (Figure 4a,c). Additionally, the 3DGM (βCD/DPU = 2/1) showed broadening of the NH-derived peak of the DPU at 6640 cm^{-1} (Figure 4b). The 3DGM (βCD/DPU = 2/1) showed the peak of the βCD-derived −OH group at 6963 cm^{-1} and a shift to 6973 cm^{-1} (Figure 4b). The 3DGM (βCD/DPU = 2/1) showed a free-water peak attributed to βCD at 5236 cm^{-1} that shifted to 5224 cm^{-1} (Figure 4d). The 3DGM (βCD/DPU = 2/1) showed a peak shift of the −OH group of βCD and free water, suggesting a decrease in free water due to the inclusion complex formation. This also

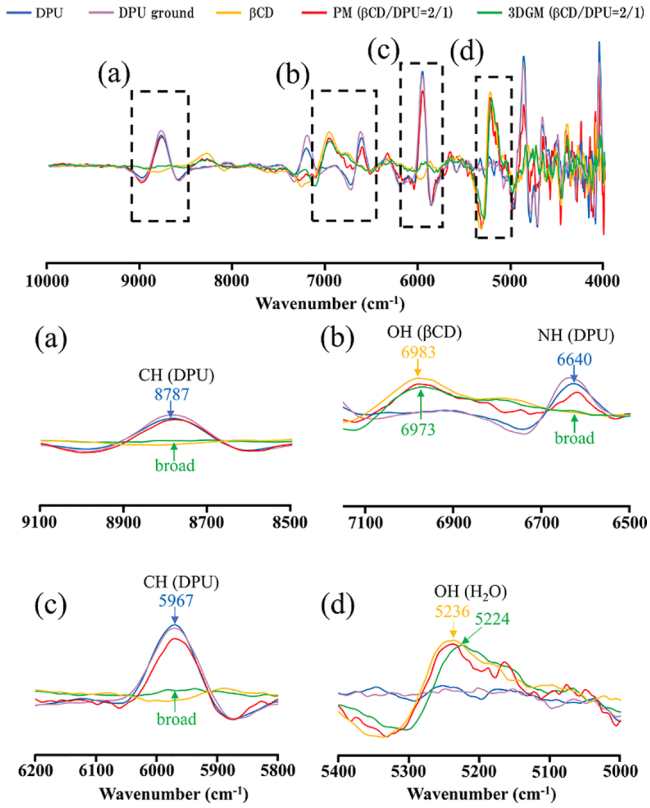

Figure 4. Second differentiation NIR absorption spectra of βCD/DPU systems. (a) 9100−8500 cm^{-1}, (b) 7100−6500 cm^{-1}, (c) 6200−5800 cm^{-1}, and (d) 5400−5000 cm^{-1}.

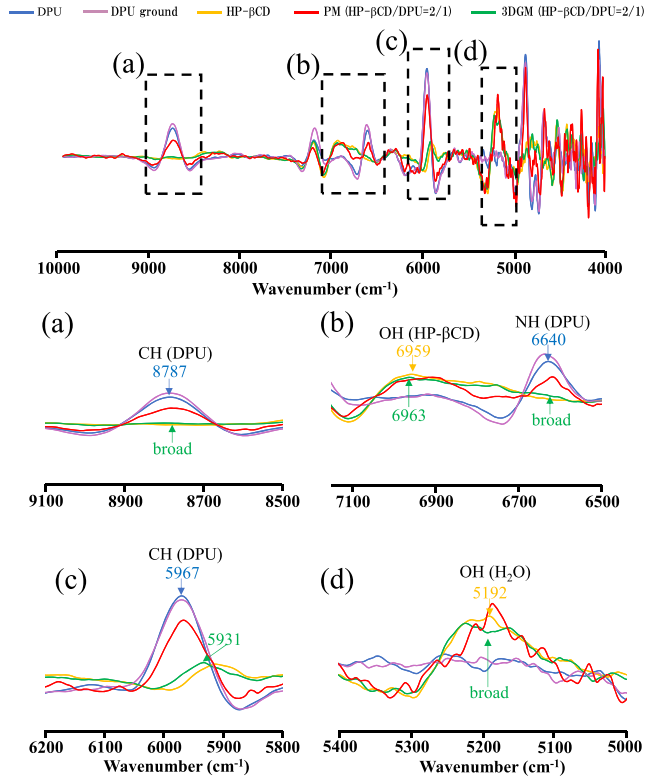

Figure 5. Second differentiation NIR absorption spectra of HP-βCD/DPU systems. (a) 9100−8500 cm^{-1}, (b) 7100−6500 cm^{-1}, (c) 6200−5800 cm^{-1}, and (d) 5400−5000 cm^{-1}.

https://doi.org/10.1021/acsomega.3c04428
ACS Omega 2023, 8, 34972−34981

indicated that intermolecular interactions were formed between the −CH and −NH groups of the benzene ring of DPU and the −OH group of βCD. In 3DGM (HP-βCD/DPU = 2/1), the CH-derived peaks of the benzene ring of DPU at 8787 and 5967 cm^{-1} broadened and shifted to 5931 cm^{-1} (Figure 5a,c). The 3DGM (HP-βCD/DPU = 2/1) showed the broadening of the NH-derived peak of DPU at 6640 cm^{-1} (Figure 5b). Furthermore, 3DGM (HP-βCD/DPU = 2/1) showed the peak derived from the −OH group of HP-βCD at 6959 cm^{-1} and a shift to 6963 cm^{-1} (Figure 5b). These findings suggested the formation of an inclusion complex in the 3DGM (HP-βCD/DPU = 2/1) owing to the intermolecular interactions between the −CH and −NH groups of the benzene ring of DPU and the −OH groups of HP-βCD.

Dissolution Test. The evaluation of solid-state physical properties confirmed the formation of inclusion complexes in the 3DGM (βCD/DPU = 2/1) and 3DGM (HP-βCD/DPU = 2/1). Therefore, to confirm the change in the DPU solubility in each inclusion complex, dissolution tests were performed using the intact DPU, PM (βCD/DPU = 2/1), PM (HP-βCD/DPU = 2/1), 3DGM (βCD/DPU = 1/1, 2/1), and 3DGM (HP-βCD/DPU = 1/1, 2/1) samples (Figure 6). The

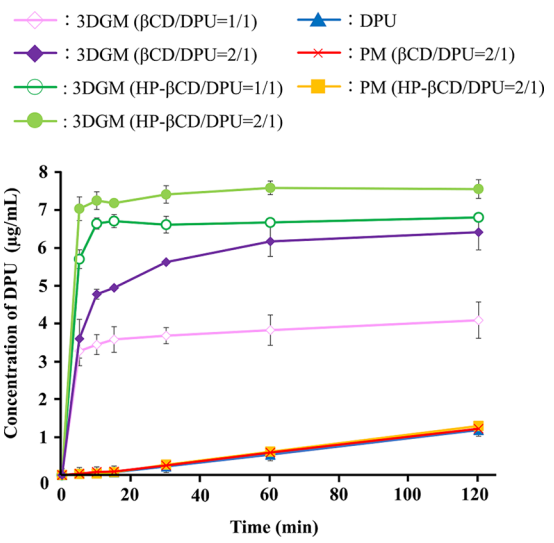

Figure 6. Dissolution profiles of DPU intact, βCD/DPU, and HP-βCD/DPU systems. Results were expressed as mean ± SD (n = 3).

dissolution concentrations of DPU in the intact DPU, PM (βCD//DPU = 2/1), and PM (HP-βCD/DPU = 2/1) samples after 5 min were low, at 0.083, 0.093, and 0.056 μg/mL, respectively. Notably, the dissolution concentrations of DPU in 3DGM (βCD/DPU = 1/1), 3DGM (βCD/DPU = 2/1), 3DGM (HP-βCD/DPU = 1/1), and 3DGM (HP-βCD/DPU = 2/1) were 3.27, 3.64, 5.70, and 7.03 μg/mL, respectively. Therefore, compared with the various PMs, the 3DGM samples exhibited solubility soon after the study was begun. In the 3DGM (βCD/DPU = 1/1), 3DGM (βCD/DPU = 2/1), 3DGM (HP-βCD/DPU = 1/1), and 3DGM (HP-βCD/DPU = 2/1), the increase in DPU solubility was attributed to the increase in the specific surface area owing to the small particle size due to milling and inclusion complex formation. In addition, the dissolution of DPU improved in both 3DGM (βCD/DPU) and 3DGM (HP-βCD/DPU) at a 2/1 molar ratio compared with that at a 1/1 molar ratio, suggesting that a 2/1 molar ratio is suitable for the βCD/DPU and HP-βCD/DPU inclusion complexes in addition to the favorable physical properties in the solid state.

^{1}H−^{1}H NOESY NMR Spectroscopy. The dissolution tests indicated improved solubility of DPU in 3DGM (βCD/DPU) and 3DGM (HP-βCD/DPU). Since the enhanced solubility could have been due to the inclusion of DPU and CDs in the solution, we performed ^{1}H−^{1}H NOESY NMR spectroscopy (Figures 7, 8, S1, and S2) to predict the intermolecular

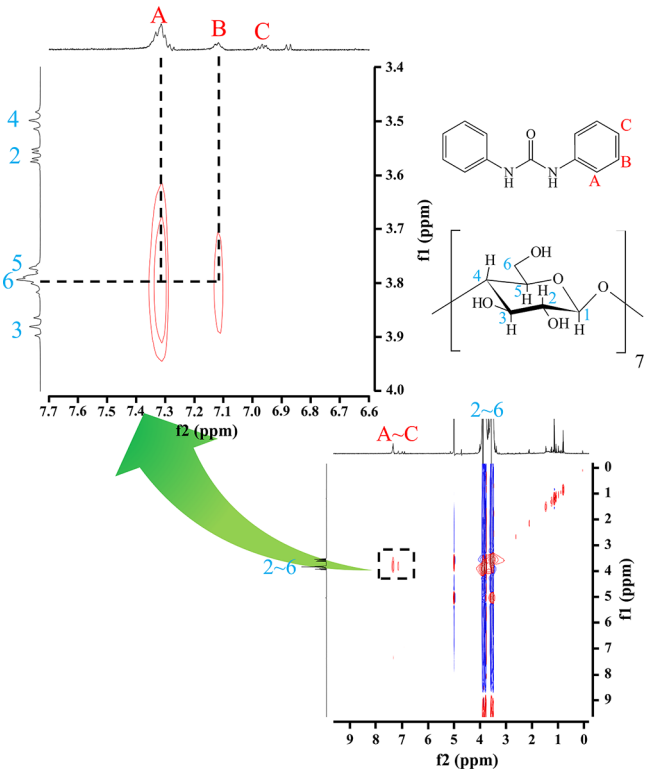

Figure 7. ^{1}H−^{1}H NOESY NMR spectra of 3DGM (βCD/DPU = 2/1) systems.

distance and relative positional relationship between DPU and CDs. The 3DGM (βCD/DPU = 1/1) showed cross-peaks between H-A (7.31 ppm) and H-B (7.11 ppm) of DPU and H-6 (3.82 ppm) in the βCD cavity (Figure S1). The 3DGM (βCD/DPU = 2/1) also showed cross-peaks between H-A (7.32 ppm) and H-B (7.12 ppm) of DPU and H-6 (3.79 ppm) in the CD cavity (Figure 7). Both 3DGM (HP-βCD/DPU = 1/1) and 3DGM (HP-βCD/DPU = 2/1) showed cross-peaks between H-A (7.32 ppm) and H-B (7.11 ppm) of DPU and H-6 (3.78 ppm) in the βCD cavity (Figures 8 and S2). Notably, NOESY NMR spectroscopy can be used to identify the protons involved in the inclusion complex of the guest molecule and CD based on cross-peaks.[35] The H-3 and H-6 protons of CD are located at the wide and narrow ring edges of CD, respectively.[36] Tachikawa et al. reported that ^{1}H−^{1}H NOESY NMR spectroscopic results showed that S-allyl cysteine in garlic forms a cross-peak with H-6 of CD, revealing an inclusion mode.[37] These results indicated that both βCD/DPU and HP-βCD/DPU are encapsulated by two molecules of CD from the narrow edge (H-6) to the wide edge (H-3), sandwiching the benzene ring of DPU. The expected inclusion modes are depicted in Figure 9. H-6 is a functional group that exists at the narrow edge of the CD, and the interaction between H-6 and DPU-derived H-a,b has been confirmed. In

https://doi.org/10.1021/acsomega.3c04428
ACS Omega 2023, 8, 34972−34981

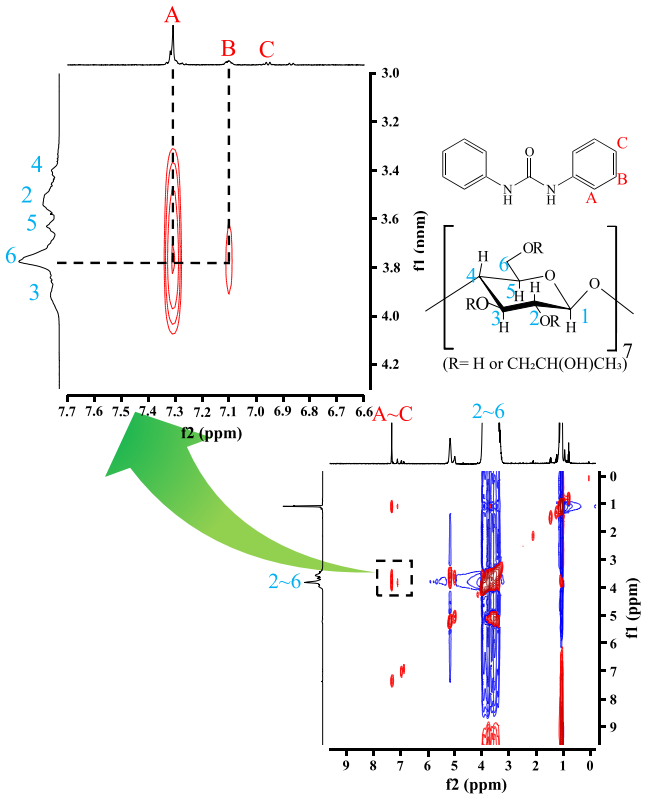

Figure 8. $^{1}H-^{1}H$ NOESY NMR spectra of 3DGM (HP-βCD/DPU = 2/1) systems.

other words, DPU (benzene ring) was encapsulated inside the CD and some of its interactions with the narrow edge of the CD were confirmed. The cross peaks with CD (H-3) and (H-6) were also confirmed, and another view is that the $^{1}H-^{1}H$ NMR NOESY spectrum shows the guest crossing the host, with one benzene group near the narrow opening and the other near H-3 at the wide mouth of the CD (both benzene groups are equal) in a 1/1 The formation of a complex can also be suggested. In addition, the phase-solubility diagram results suggest a possible 1/1 molar ratio in the solution state. In other words, NMR measurements suggest that when 3DGM is dispersed in water, the inclusion in the solid state reflects the inclusion environment, and in the dissolution test, CDs/DPU forms the inclusion ratio molar ratios (CDs/DPU = 2/1 and 1/1). Therefore, the improved dissolution of 3DGM (CDs/DPU = 2/1) compared to 3DGM (CDs/DPU = 1/1) in the dissolution test may also be due to factors that improve the dissolution. The presence of water is essential for the formation of inclusion complexes even in the solid state, and mechanochemical effects may contribute to the formation of inclusion complexes in this study. The mechanochemical reaction between organic substances may be related to the ease of deformation of the van der Waals crystals. When CDs and organic drugs are mixed and ground, strong hydrogen bonds are formed between them, leading to the inclusion of CDs. In the present study, the inclusion molar ratio in solution (CDs/DPU = 1/1) and in the solid state (CDs/DPU = 2/1) is considered to be affected by this mechanochemical effect. The inclusion mode for the CDs/DPU inclusion molar ratio of 1/1 is shown in Figure S3.

Effects of CDs/DPU on Plant Growth. Previous physicochemical evaluations have shown that (1) solid

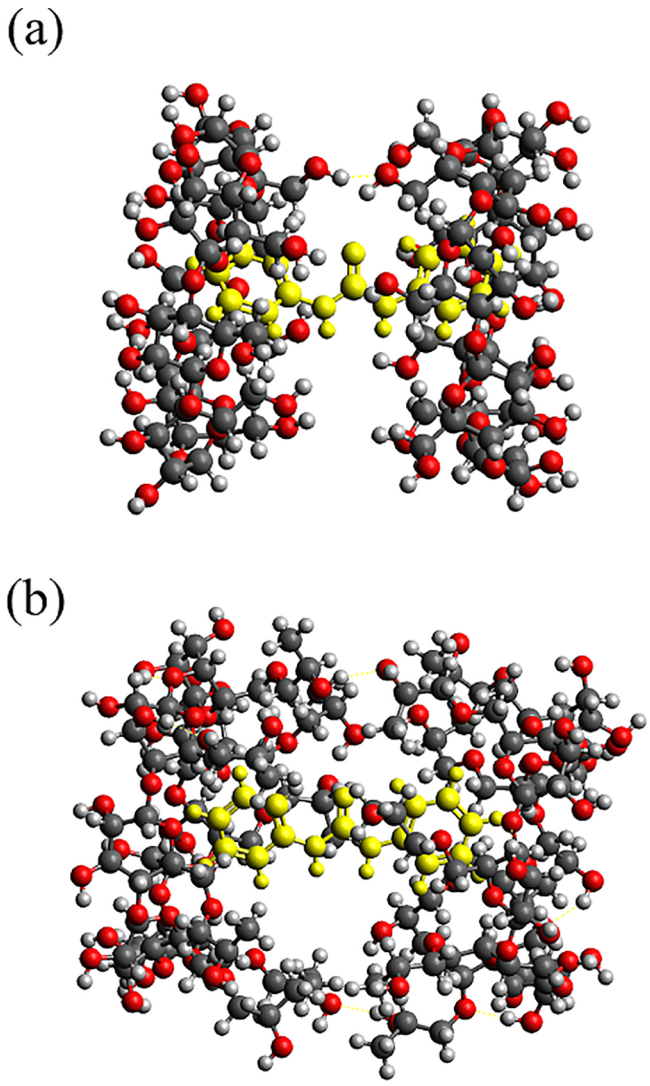

Figure 9. Image of proposed structure images of βCD/DPU and HP-βCD/DPU complex. (a) 3DGM (βCD/DPU = 2/1) and (b) 3DGM (HP-βCD/DPU = 2/1).

dispersions were prepared by 3DGM and the preparation of CDs/DPU complexes was confirmed, (2) solubility of DPU was improved by the formation of CDs/DPU complex, and (3) it was inferred that the CDs/DPU complex is in a different inclusion molecular state in the solid state and in solution. Therefore, we considered it necessary to examine the plant growth assay of the CDs/DPU complex using broccoli sprouts as a model plant. DPU is a cytokinin with plant growth-promoting activity.[8] To confirm the plant growth-promoting effect of DPU via the formation of βCD/DPU and HP-βCD/DPU inclusion complexes, the intact DPU, intact βCD, intact HP-βCD, 3DGM (βCD/DPU = 2/1), 3DGM (HP-βCD/DPU = 2/1), 3DGM (βCD/DPU = 1/1), and 3DGM (HP-βCD/DPU = 1/1) samples were used to grow broccoli sprouts. Distilled water was used as a control (Figures 10 and 11). There was no difference in the length of broccoli sprouts among the control, intact βCD, and intact HP-βCD. In contrast, intact DPU, 3DGM (βCD/DPU = 2/1), 3DGM (HP-βCD/DPU = 2/1), 3DGM (βCD/DPU = 1/1), and 3DGM (HP-βCD/DPU = 1/1) plants were shorter than the control plants 5 days after seeding (Figure 10a). The thickness of broccoli sprouts showed no difference among the control,

https://doi.org/10.1021/acsomega.3c04428
ACS Omega 2023, 8, 34972−34981

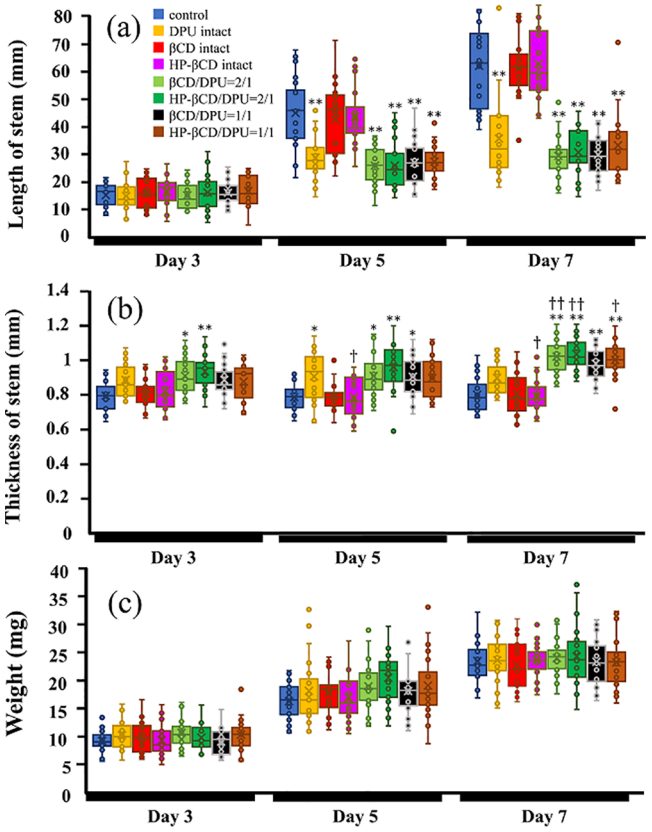

Figure 10. Effect of DPU on broccoli sprouts over a period of 7 days. (a) Length of stem, (b) thickness of stem, and (c) weight of the broccoli sprouts. *:$p < 0.05$, **:$p < 0.01$ vs control, †:$p < 0.05$, and ††: $p < 0.01$ vs DPU intact (Tukey's test).

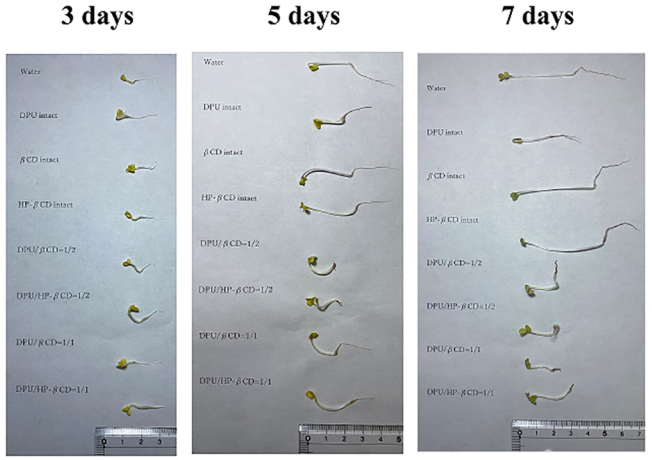

Figure 11. Observation of broccoli sprouts each sample on 7 days.

DPU intact, βCD intact, and intact HP-βCD groups (Figure 10b). Notably, the 3DGM (HP-βCD/DPU = 2/1) was thicker than the control 3 days after seeding and the 3DGM (βCD/DPU = 2/1), 3DGM (βCD/DPU = 1/1), and 3DGM (HP-βCD/DPU = 1/1) 7 days after seeding. The weight of the broccoli sprouts did not differ in any of the samples compared with that of the control (Figure 10c). Notably, the DPU is an agonist that acts on the analogous site of adenine-type cytokinins, as described by Iwamura et al. It exhibits cytokinin activity by ligand binding via hydrogen bonding of −NH groups and hydrophobic interactions at the benzene ring.[38] Further, the stability constant of the adamantane/insulin conjugate-PEG-βCD complex is 1.0×10^4 M^{-1}, indicating high affinity without dissociation of the complex in blood.[39] In contrast, the stability constants of βCD/DPU and HP-βCD/DPU calculated using the phase-solubility diagrams in this study were not high and can exist in solution without a CD molecule and with an exposed −NH group and benzene ring of the active site (e.g., molar ratio = 2/1 and 1/1 coexisting). The CD1 molecule was removed in the solution state. These results suggest that βCD/DPU and HP-βCD/DPU inclusion complexes in the solution state could bind to the receptors exhibiting cytokinin activity and exert a biochemical influence on broccoli sprouts during fruiting. In addition, the hydrogen bonding of the −OH group of the one-molecule CD involved in the inclusion with the cytokinin-activated receptor may provide further robust ligand binding. This could account for the difference in the cytokinin activity of the intact DPU, βCD/DPU, and HP-βCD/DPU inclusion complexes in the fructification of the plants.

Overall, these results suggested that the intact DPU not only improved the solubility of DPU but also had some effect on plant growth via the formation of inclusion complexes with βCD and HP-βCD. In the future, it will be a challenge to elucidate the genetic engineering predisposition of how inclusion complexes are attributed to plant growth factors.

CONCLUSIONS

In this study, the formation of βCD/DPU and HP-βCD/DPU inclusion complexes was confirmed using 3DGM. The use of 3D ball milling enabled the preparation of inclusion complexes using only reagents and not solvents, which improved the solubility of the DPU in 3DGM (βCD/DPU = 2/1) and 3DGM (HP-βCD/DPU = 2/1). In addition, the plant growth-promoting effects of DPU were significant in the 3DGM (βCD/DPU) and 3DGM (HP-βCD/DPU) groups. This is expected to improve the handling of DPU and expand its application in various fields, including its use as a plant growth agent. Investigating the preparation of inclusion complexes in future studies using CDs combined with other DPU derivatives, such as phenyl urea-type cytokinins, is necessary. We performed a plant growth assay of CDs/DPU complexes using broccoli sprouts as a model plant and obtained unique findings. In the future, the involvement of CDs/DPU in plant growth should be examined in detail from an intracellular pharmacological perspective.

MATERIALS AND METHODS

Materials. The DPU (lot GQ6WG-RD) was purchased from Tokyo Chemical Industry Co., Ltd. (Tokyo, Japan) (Figure 12a). The βCD and HP-βCD (hydroxypropyl chain substitutions 0.6−0.9) were provided by Cyclo Chem Bio Co., Ltd., Kobe, Japan), and the βCD was stored at 40 °C and a relative humidity of 82% for 7 days (Figure 12b,c). Deuterium oxide (D_2O, 99.9%) was used as the NMR solvent, and other reagents were obtained from Wako Pure Chemical Industries Ltd. (Osaka, Japan).

Preparation of PMs and 3DGM. The PMs of DPU (37.1 mg)/βCD (462.9 mg) and DPU (34.36 mg)/HP-/βCD (465.64 mg) each in a 1/2 molar ratio were prepared and mixed in a vortex mixer for 1 min. The 3DGMs of DPU, βCD, and HP-βCD were prepared by grinding 500 mg of the PMs (βCD/DPU and HP-βCD/DPU) using a 3D ball mill (3D-80,

https://doi.org/10.1021/acsomega.3c04428
ACS Omega 2023, 8, 34972−34981

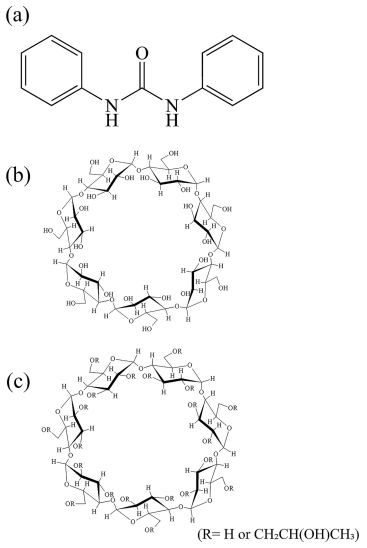

Figure 12. Chemical structure of DPU, βCD, and HP-βCD. (a) 1.3-Diphenylurea, (b) βCD, and (c) HP-βCD.

Nagao System Inc., Tokyo, Japan) with a 96 g ball (ZrO_2), ⌀5 mm, for 60 min.

Methods. *Phase-Solubility Diagrams.* The phase-solubility diagrams were drawn based on the method described by Higuchi et al.[26] Excess DPU (50 mg) was added to 10 mL of each solution of βCD (0−50 mM) or HP-βCD (0−50 mM) and then shaken at 100 rpm (25 ± 0.5 °C) for 24 h using a medium-sized constant-temperature shaker BR42FL, TAITEC (Saitama, Japan). The suspension obtained by shaking was filtered through a 0.45 μm membrane filter DISMIC 25AS, ADVANTEC (Tokyo, Japan), and the filtrate was diluted with distilled water/acetonitrile in a ratio of 2/3 and measured using high-performance liquid chromatography (HPLC). The obtained phase-solubility diagrams were used to calculate the apparent stability constants of CDs/DPU at molar ratios of 1/1 and 2/1 ($K_{1/1}$ and $K_{2/1}$) according to Higuchi and Connor's equations[27]:

$$\mathrm{KS} = \mathrm{slope}/S_0 \cdot (1 - \mathrm{slope}) \quad (1)$$

$$S_{\mathrm{tot}} = S_0 + K_{1/1} \cdot S_0[\mathrm{CD}] + K_{1/1} \cdot K_{2/1} \cdot S_0 \cdot [\mathrm{CD}]^2 \quad (2)$$

where S_0 is the solubility of DPU in the absence of CD, S_{tot} is the total concentration of DPU, and [CD] is the free concentration of CD.

The CE of the relationship between the drug and the CD forming a complex with a molar ratio of 1/1 was calculated using the following formula:

$$\mathrm{CE} = [\mathrm{Drug/CD}]/[\mathrm{CD}] = S_0 \cdot K_{1/1} = \mathrm{slope}/(1 - \mathrm{slope}) \quad (3)$$

Quantification of DPU Using HPLC. Samples were quantified by using an HPLC system (Shimadzu Co., Kyoto, Japan) equipped with a pump (LC-20ADvp). The concentration of DPU was measured at an absorption wavelength of 257 nm. The Inertsil ODS-3 column (⌀5 μm 4.6 × 150 mm) with a sample injection volume of 30 μL was used at a column temperature of 40 °C. The mobile phase was distilled water/acetonitrile (2/3), and the DPU retention time was set to 8 min.

PXRD. The measurements were performed by using a powder X-ray diffractometer (Miniflex II, Rigaku, Tokyo, Japan). For PXRD, Cu rays (30 kV, 15 mA) were used as the X-rays, with scanning conditions of 4°/min, a sampling width of 0.02°, a scanning speed of 3.00 s, and a measurement range of 2θ = 3−40°. The powder samples were placed on a glass plate, such that the sample plane was flat for measurement.

DSC. A high-sensitivity DSC (Thermo Plus Evo, Rigaku, Tokyo, Japan) was used. The samples (2 mg) were placed in an aluminum pan and measured under nitrogen gas flow (60 mL/min) with a temperature increase rate of 10 °C/min in the measurement range of 50−330 °C.

NIR Absorption Spectrum. The UV−vis-NIR spectrophotometer (V770 EX; JASCO, Tokyo, Japan) was used. The measurement range was 1000−4000 cm^{-1} with a resolution of 8 cm^{-1} at 25 °C. Approximately 3 mg of each sample was loaded into a fine powder cell, and measurements were performed at an optical path spacing of 2 nm. The obtained spectra were then subjected to second-order differentiation.

Dissolution Test. The dissolution test was conducted using a dissolution tester (NTR-593; Toyama Sangyo, Osaka, Japan) in accordance with the dissolution test paddle method of the JP18 revision. It was performed in 900 mL of distilled water (37 ± 0.5 °C) stirred at 50 rpm. Next, 20 mg of DPU was accurately weighed and placed in a paddle. Thereafter, 10 mL of dissolved sample was collected at 5, 10, 15, 30, 60, and 120 min and filtered through a 0.45 μm membrane filter (DISMIC 25AS, ADVANTEC, Tokyo, Japan). To maintain a constant volume of the solution, the same temperature and volume of the solution were used after each sample was collected. The filtrate was diluted with distilled water/acetonitrile in a ratio of 2/3 and analyzed using HPLC.

^{1}H−^{1}H NOESY NMR Spectroscopy. An NMR system (AVANCE NEO 600 system, Bruker, Kanagawa, Japan) was used, with D_2O as the solvent. The 1H chemical shift was based on the residual D_2O signal (4.63 ppm). The resonance frequency was 600.1 MHz, pulse width 8.00 μs, relaxation time 0.800 s, and integration frequency 1024 at 25 °C.

Cultivation of Broccoli Sprouts. The broccoli sprout cultivation kit (Vegetable Garden Club, Mie, Japan) was used for the cultivation experiment. Five hundred seeds were sown and grown in the dark at 20 ± 2 °C and a humidity of 47 ± 2%. The length, thickness, and weight of the broccoli sprouts were measured 3, 5, and 7 days after seeding.

Statistical Analysis. Comparisons of experimental groups were evaluated using the Tukey test and one-way analysis of variance multiple comparison test, with $p < 0.05$ indicating a significant difference.

■ ASSOCIATED CONTENT

Supporting Information

The Supporting Information is available free of charge at https://pubs.acs.org/doi/10.1021/acsomega.3c04428.

Regarding DPU and CDs in the solution, ^{1}H−^{1}H NOESY NMR spectroscopy, and image of proposed structure images of βCD/DPU and HP-βCD/DPU complex (PDF)

■ AUTHOR INFORMATION

Corresponding Author

Yutaka Inoue − *Laboratory of Nutri-Pharmacotherapeutics Management, Faculty of Pharmacy and Pharmaceutical Sciences, Josai University, Sakado, Saitama 3500295, Japan;*

https://doi.org/10.1021/acsomega.3c04428
ACS Omega 2023, 8, 34972−34981

orcid.org/0000-0003-3419-343X; Phone: +81-49-271-7980; Email: yinoue@josai.ac.jp; Fax: +81-49-271-7980

Authors

Koki Yamamoto − *Laboratory of Nutri-Pharmacotherapeutics Management, Faculty of Pharmacy and Pharmaceutical Sciences, Josai University, Sakado, Saitama 3500295, Japan*

Takashi Tanikawa − *Laboratory of Nutri-Pharmacotherapeutics Management, Faculty of Pharmacy and Pharmaceutical Sciences, Josai University, Sakado, Saitama 3500295, Japan*

Junki Tomita − *Instrument Analysis Center, Josai University, Sakado, Saitama 3500295, Japan*

Yoshiyuki Ishida − *CycloChem Bio Co., Ltd., Kobe 6500047, Japan*

Daisuke Nakata − *CycloChem Bio Co., Ltd., Kobe 6500047, Japan*

Keiji Terao − *CycloChem Bio Co., Ltd., Kobe 6500047, Japan*

Complete contact information is available at: https://pubs.acs.org/10.1021/acsomega.3c04428

Notes

The authors declare no competing financial interest.

■ ACKNOWLEDGMENTS

The authors are grateful to Cyclo Chem Bio Co. Ltd. for providing the CD samples. The authors are thankful to the members of the Nutrition and Pharmacotherapy Management Laboratory for washing the laboratory instruments used in the study.

■ ABBREVIATIONS

DPU	1,3-diphenylurea
αCD	α-cyclodextrin
βCD	β-cyclodextrin
γCD	γ-cyclodextrin
HP-βCD	2-hydroxypropyl-β-cyclodextrin
PM	physical mixture
3DGM	three-dimensional ground mixture
PXRD	powder X-ray diffraction
DSC	differential scanning calorimetry
IR	infrared
NIR	near infrared
NOESY	nuclear overhauser effect spectroscopy
HPLC	high-performance liquid chromatography

■ REFERENCES

(1) Bozsó, Z.; Barna, B. Diverse effect of two cytokinins, kinetin and benzyladenine, on plant development, biotic stress tolerance, and gene expression. *Life* **2021**, *11*, 1404.

(2) Shan, T.; Zhang, X.; Guo, C.; Guo, S.; Zhao, X.; Yuan, Y.; Yue, T. Identity, synthesis, and cytotoxicity of forchlorfenuron metabolites in kiwifruit. *J. Agric. Food. Chem.* **2021**, *69*, 9529−9535.

(3) Kieber, J. J.; Schaller, G. E. Cytokinins. *Arabidopsis Book* **2014**, *12*, No. e0168.

(4) Koprna, R.; De Diego, N.; Dundálková, L.; Spíchal, L. Use of cytokinins as agrochemicals. *Bioorg. Med. Chem.* **2016**, *24*, 484−492.

(5) Werner, T.; Schmülling, T. Cytokinin action in plant development. *Curr. Opin. Plant Biol.* **2009**, *12*, 527−538.

(6) Khan, A. S.; Ali, S. *Preharvest sprays affecting shelf life and storage potential of fruits*. In *Preharvest Modulation of Postharvest Fruit and Vegetable Quality*; Sidiqqui, M. W., Ed.; Academic Press Inc.: Cambridge, MA, USA, 2018; pp. 209−255.

(7) Valverde, A.; Piedra, L.; Aguilera, A.; Boulaid, M.; Camacho, F. Analysis and residue levels of forchlorfenuron (CPPU) in watermelons. *J. Environ. Sci. Health B* **2007**, *42*, 801−807.

(8) Nisler, J.; Kopečný, D.; Končitíková, R.; Zatloukal, M.; Bazgier, V.; Berka, K.; Zalabák, D.; Briozzo, P.; Strnad, M.; Spíchal, L. Novel thidiazuron-derived inhibitors of cytokinin oxidase/dehydrogenase. *Plant Mol. Biol.* **2016**, *92*, 235−248.

(9) Sliwinska-Kowalska, M. Organic solvent exposure and hearing loss. *Occup. Environ. Med.* **2008**, *65*, 222−223.

(10) Schenker, M. B.; Jacobs, J. A. Respiratory effects of organic solvent exposure. *Tuber. Lung. Dis.* **1996**, *77*, 4−18.

(11) Baker, E. L. Organic solvent neurotoxicity. *Annu. Rev. Public Health.* **1988**, *9*, 223−232.

(12) Wüpper, S.; Lüersen, K.; Rimbach, G. Cyclodextrins, natural compounds, and plant bioactives-a nutritional perspective. *Biomolecules.* **2021**, *11*, 401.

(13) Patel, M.; Hirlekar, R. Multicomponent cyclodextrin system for improvement of solubility and dissolution rate of poorly water soluble drug. *Asian J. Pharm. Sci.* **2019**, *14*, 104−115.

(14) Inoue, Y.; Nanri, A.; Arce, F. J.; See, G. L.; Tanikawa, T.; Yokogawa, T.; Kitamura, M. Preparation and spectroscopic characterization of ternary inclusion complexes of ascorbyl palmitate and urea with γ-cyclodextrin. *Chem. Eng.* **2023**, *7*, 29.

(15) Sid, D.; Baitiche, M.; Elbahri, Z.; Djerboua, F.; Boutahala, M.; Bouaziz, Z.; Le Borgne, M. Solubility enhancement of mefenamic acid by inclusion complex with β-cyclodextrin: in silico modelling, formulation, characterisation, and in vitro studies. *J. Enzym. Inhib. Med. Chem.* **2021**, *36*, 605−617.

(16) Kogawa, A. C.; Zoppi, A.; Quevedo, M. A.; Nunes Salgado H, R.; Longhi, M. R. Increasing doxycycline hyclate photostability by complexation with β-cyclodextrin. *AAPS PharmSciTech* **2014**, *15*, 209−1217.

(17) D'Aria, F.; Pagano, B.; Giancola, C. Thermodynamic properties of hydroxypropyl-β-cyclodextrin/guest interaction: A survey of recent studies. *J. Therm. Anal. Calorim.* **2022**, *147*, 4889−4897.

(18) Stasiłowicz, A.; Tykarska, E.; Lewandowska, K.; Kozak, M.; Miklaszewski, A.; Kobus-Cisowska, J.; Szymanowska, D.; Plech, T.; Jenczyk, J.; Cielecka-Piontek, J. Hydroxypropyl-β-cyclodextrin as an effective carrier of curcumin - piperine nutraceutical system with improved enzyme inhibition properties. *J. Enzyme Inhib. Med. Chem.* **2020**, *35*, 1811−1821.

(19) Raval, M.; Bagada, H. Formulation and evaluation of cyclodextrin-based thermosensitive in situ gel of azithromycin for periodontal delivery. *J. Pharm. Innov.* **2021**, *16*, 67−84.

(20) Inoue, Y.; Hirano, A.; Murata, I.; Kobata, K.; Kanamoto, I. Assessment of the physical properties of inclusion complexes of forchlorfenuron and γ-cyclodextrin derivatives and their promotion of plant growth. *ACS Omega* **2018**, *3*, 13160−13169.

(21) Jicsinszky, L.; Rossi, F.; Solarino, R.; Cravotto, G. Comparison of the Conventional and Mechanochemical Syntheses of Cyclodextrin Derivatives. *Molecules* **2023**, *28*, 467.

(22) Shiozawa, R.; Inoue, Y.; Murata, I.; Kanamoto, I. Effect of antioxidant activity of caffeic acid with cyclodextrins using ground mixture method. *Asian J. Pharm. Sci.* **2018**, *13*, 24−33.

(23) *3D Ball Mill (3D Reactor)*; Nagao System, Inc. URL: https://www.youtube.com/watch?v=d4WAZl4GVJw.

(24) Inoue, Y.; Shigematsu, M.; Komatsu, T.; Oguchi, T.; Arce, F. J.; See, G. L. Preparation and spectroscopic characterization of inclusion complexes of 3d ball-milled rifampicin with β-cyclodextrin and γ-cyclodextrin: 3d ball-milled rifampicin with β-cyclodextrin and γ-cyclodextrin. *AAPS PharmSciTech* **2022**, *23*, 138.

(25) Inoue, Y.; Osada, M.; Murata, I.; Kobata, K.; Kanamoto, I. Evaluation of Solubility Characteristics of a Hybrid Complex of Components of Soy. *ACS Omega* **2019**, *16*, 8632−8640.

(26) Loftsson, T.; Sigurdsson, H. H.; Jansook, P. Anomalous properties of cyclodextrins and their complexes in aqueous solutions. *Materials* **2023**, *16*, 2223.

(27) Higuchi, T.; Connors, K. A.*Phase Solubility Techniques*; Advances in Chemical Instrumentation; 1965 ; pp. 117−212.

(28) Loftsson, T.; Másson, M.; Brewster, M. E. Self-Association of cyclodextrins and cyclodextrin complexes in aquwous solutions. *Int. J. Pharm. Sci.* **2019**, *560*, 228−234.
(29) Yang, L. V. J.; Xia, S.; Ma, S. VX; Zhou, S. VY; Zhao, X. Q.; Hui, Wang S.; Li, M. Y.; Yang, X. D. Host-guest system of hesperetin and β-cyclodextrin or its derivatives: Preparation, characterization, inclusion mode, solubilization and stability. *Mater. Sci. Eng. C* **2016**, *59*, 1016−1024.
(30) Hirotsu, T.; Higashi, T.; Hashim, I. I. A.; Misumi, S.; Wada, K.; Motoyama, K.; Arima, H. Self-assembly PEGylation retaining activity (SPRA) technology via a host-guest interaction surpassing conventional PEGylation methods of proteins. *Mol. Pharmaceutics* **2017**, *14*, 368−376.
(31) Iwata, M.; Fukami, T.; Kawashima, D.; Sakai, M.; Furuishi, T.; Suzuki, T.; Tomono, K.; Ueda, H. Effectiveness of mechanochemical treatment with cyclodextrins on increasing solubility of glimepiride. *Pharmazie* **2009**, *64*, 390−394.
(32) Inoue, Y.; Watanabe, S.; Suzuki, R.; Murata, I.; Kanamoto, I. Evaluation of actarit/γ-cyclodextrin complex prepared by different methods. *J. Incl. Phenom. Macrocycl. Chem.* **2015**, *81*, 161−168.
(33) Nisar, T.; Wang, Z. C.; Yang, X.; Tian, Y.; Iqbal, M.; Guo, Y. Characterization of citrus pectin films integrated with clove bud essential oil: Physical, thermal, barrier, antioxidant and antibacterial properties. *Int. J. Biol. Macromol.* **2018**, *106*, 670−680.
(34) Inoue, Y.; Yoshida, M.; Ezawa, T.; Tanikawa, T.; Arce, F., Jr.; See, G. L.; Tomita, J.; Suzuki, M.; Oguchi, T. Inclusion complexes of daidzein with cyclodextrin-based metal-organic framework-1 enhance its solubility and antioxidant capacity. *AAPS PharmSciTech* **2021**, *23*, 2.
(35) Tárkányi, G.; Németh, K.; Mizsei, R.; Töke, O.; Visy, J.; Simonyi, M.; Jicsinszky, L.; Szemán, J.; Szente, L. Structure and stability of warfarin-sodium inclusion complexes formed with permethylated monoamino-β-cyclodextrin. *J. Pharm. Biomed. Anal.* **2013**, *72*, 292−298.
(36) Del Valle, E. M. M. Cyclodextrins and their uses: a review. *Process Biochem.* **2004**, *39*, 1033−1046.
(37) Tachikawa, R.; Saito, H.; Moteki, H.; Kimura, M.; Kitagishi, H.; Arce, F., Jr.; See, G. L.; Tanikawa, T.; Inoue, Y. Preparation, characterization, and in vitro evaluation of inclusion complexes formed between S-allylcysteine and cyclodextrins. *ACS Omega* **2022**, *7*, 31233−31245.
(38) Iwamura, H.; Murakami, S.; Koshimizu, K.; Matsubara, S. Quantitative structure-activity relationships in cytokinin agonistic and antagonistic pyrido[2,3-d]pyrimidine derivatives: insights into receptor topology. *J. Med. Chem.* **1985**, *28*, 577−83.
(39) Hirotsu, T.; Higashi, T.; Abu Hashim, I. I.; Misumi, S.; Wada, K.; Motoyama, K.; Arima, H. Self-assembly PEGylation retaining activity (spra) technology via a host-guest interaction surpassing conventional PEGylation methods of proteins. *Mol. Pharmaceutics* **2017**, *14*, 368−376.

https://doi.org/10.1021/acsomega.3c04428
ACS Omega 2023, 8, 34972−34981